Werk

Jahr: 1984
Kollektion: fid.geo
Signatur: 8 Z NAT 2148:54
Digitalisiert: Niedersächsische Staats- und Universitätsbibliothek Göttingen
Werk Id: PPN1015067948_0054
PURL: http://resolver.sub.uni-goettingen.de/purl?PPN1015067948_0054

LOG Id: LOG_0026
LOG Titel: Restoration of broad-band seismograms (Part I)
LOG Typ: article

Übergeordnetes Werk

Werk Id: PPN1015067948
PURL: http://resolver.sub.uni-goettingen.de/purl?PPN1015067948
OPAC: http://opac.sub.uni-goettingen.de/DB=1/PPN?PPN=1015067948

Contact

Niedersächsische Staats- und Universitätsbibliothek Göttingen
Georg-August-Universität Göttingen
Platz der Göttinger Sieben 1
37073 Göttingen
Germany
Email: gdz@sub.uni-goettingen.de

J Geophys (1984) 54: 114–122

Journal of Geophysics

Restoration of broad-band seismograms (Part I)

D. Seidl[1] **and W. Stammler**[2]

[1] Seismologisches Zentralobservatorium Gräfenberg, Krankenhausstr. 1, D-8520 Erlangen, FRG
[2] Lehrstuhl für Nachrichtentechnik, Cauerstr. 7, D-8520 Erlangen, FRG

Abstract. Restoration includes all steps of seismogram processing applied in the time or frequency domain to compensate for the signal distortion caused by the seismograph. Restoration of broad-band seismograms is demonstrated using recordings of the Graefenberg (GRF) array. For this purpose a comprehensive description of the characteristics of the GRF seismograph system in the time and frequency domain is presented.

To investigate signal distortions and the effectiveness of restoration algorithms, a program for the digital simulation of a wide class of seismograph systems is described. Using some theorems about first arrival time and first motion sign of a wavelet, the accuracy of arrival time measurements as well as the determination of first motion signs are discussed and illustrated.

Key words: Restoration – Broad-band seismogram – Graefenberg array – Digital simulation – Arrival time – First motion sign

Introduction

Restoration as described here includes all steps of seismogram processing in time or frequency domain applied to compensate for the signal distortion caused by the seismograph system. In general, an exact recovery of the input signal from the output response of a linear causal system is possible for systems which are strictly minimum-delay, that is, all zeros of the transfer function lie in the open left s-plane (Robinson, 1962). Since the transfer function of a seismometer with a pendulum sensor has a multiple zero at $s=0$ and due to nonlinearities, instrument noise and limited resolution of the seismograph and recording system, the true ground motion can be recovered only approximately. Two approaches are usually applied: band-limited restoration of seismogram segments in digital processing and correction of single seismogram parameters in the usual domain analysis of analog seismograms. Both methods exhibit some special features for digital wide-band feedback seismograph systems.

In digital processing a band-limited restoration can be performed by dividing the complex seismogram spectrum by the gain-and-phase characteristics of the seismograph system. This compensates only for the linear distortions. Since the signal distortion due to the nonlinear behavior of the mechanical sensor is strongly reduced in a feedback seismometer of the force-balance type, a wide-band recovery of the spectrum or signal form of true ground motion is possible over a larger range of amplitudes. The degree of approximation is limited mainly by the low frequency instrument noise and by the resolution of the recording system. Applications of wide-band restoration are, for example, the interpretation of broad-band recordings with theoretical seismograms or the determinations of displacement pulse area (proportional to source moment) and velocity pulse energy (proportional to radiated energy).

In the usual time domain analysis of analog seismograms, only a correction of single seismogram parameters can be performed. Examples are the estimation of narrow-band spectral amplitudes for magnitude determination and the correction of group-delay or phase-delay in the dispersion analysis of narrow-band surface wave groups. For standard time domain analysis broad-band seismograms must usually be prefiltered. This improves the signal-to-noise ratio for signal detection and arrival time measurement and enhances the spectral amplitudes in the conventional short and long period frequency bands used for magnitude determinations. To avoid a bias in magnitude due to improper equalization of the prefilter response, simulation filters (Seidl, 1980) for standard seismograph systems can be applied in place of simple band pass filters.

This paper is the first of two dealing with the restoration of Graefenberg broad-band seismograms.

Paper I describes the frequency and time domain characteristics of the Graefenberg seismograph system. To investigate linear distortions and the effectiveness of restoration algorithms a program for the digital simulation of seismograph systems is presented. Some theorems about arrival time and first motion sign of signals are discussed and illustrated.

Paper II (in preparation) is concerned with the wide-band recovery of true ground motion and with the determination of narrow-band spectral amplitudes (magnitudes), displacement pulse area (source moment) and pulse energy (radiated energy) in time or frequency domain.

Offprint requests to: D. Seidl

Frequency and time domain characteristics of the Graefenberg seismograph system

The seismograph system of the Graefenberg array (Harjes and Seidl, 1978) consists of the feedback seismometer STS-1 (Wielandt and Streckeisen, 1982) and an antialiasing filter. The seismometer has two outputs: a broad-band (BB) output proportional to ground velocity and an integrated long period (LP) output proportional to ground displacement. The transfer function of the BB-output for ground velocity is therefore the same as the transfer function of the LP-output for ground displacement.

The transfer function of the BB-output for velocity is given by

$$H_S(s)=\frac{G_0\cdot s^2}{s^2+2h_0\omega_0 s+\omega_0^2}\cdot\frac{(s+a_1)\omega_1^2}{s^2+2h_1\omega_1 s+\omega_1^2}. \tag{1}$$

The gain factor G_0 ($G_{0\,BB}=2{,}400$ V s/m for the BB-output and $G_{0\,LP}=780$ V/m for the LP-output respectively) is omitted in the following formulas. The BB-output is used for the array data acquisition system with sampling rate $f_S=20$ Hz, the LP-output is recorded for selected channels with $f_S=0.1$ Hz.

The first factor in Eq. (1) corresponds to the transfer function of a conventional seismometer. The denominator of the second factor can replace one stage of an antialiasing filter, when the zero at $s=-a_1$ in the numerator (caused by the resistance of the feedback coil in the differential path) is cancelled by an additional pole in the transfer function of the antialiasing filter.

The transfer function of the antialiasing filter used is

$$H_F(s)=\frac{1}{s+a_1}\cdot\frac{\omega_1}{s+\omega_1}\prod_{k=2}^{3}\frac{\omega_1^2}{s^2+2h_k\omega_1 s+\omega_1^2}. \tag{2}$$

The overall transfer function of the seismograph system becomes

$$H(s)=H_0(s)\cdot H_1(s) \tag{3}$$

where

$$H_0(s)=\frac{s^n}{s^2+2h_0\omega_0 s+\omega_0^2}$$

and

$$H_1(s)=\frac{\omega_1}{s+\omega_1}\prod_{k=1}^{3}\frac{\omega_1^2}{s^2+2h_k\omega_1 s+\omega_1^2}.$$

Therefore, the seismograph system can be considered to be a conventional seismometer with transfer function $H_0(s)$ in series with a 7-th order Butterworth antialiasing filter with transfer function $H_1(s)$. The relationship of output to input as determined by the exponent n in the transfer function $H(s)$ is as follows:

Input \ Output	BB	LP
DIS	$n=3$	$n=2$
VEL	$n=2$	$n=1$
ACC	$n=1$	$n=0$

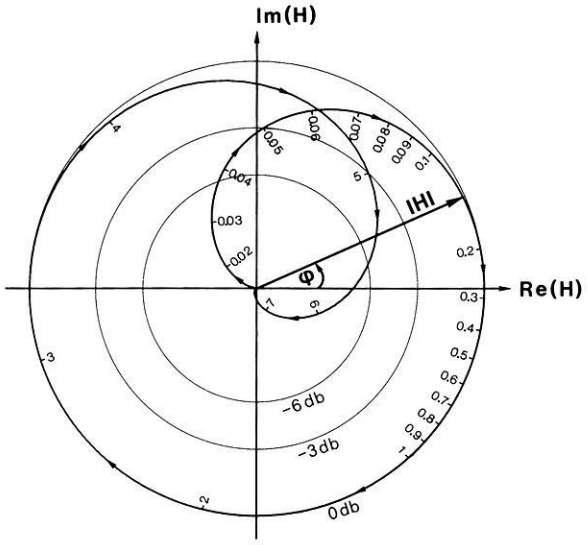

Fig. 1. Polar diagram of the complex gain-and-phase vector $|H(j\omega)|\cdot\exp(j\varphi(\omega))$ of BB-output for ground velocity or LP-output for ground displacement of the Graefenberg seismograph system. The numbers indicate frequencies in Hz. Circles are drawn for the attenuations 0 db (pass band), 3 db and 6 db, respectively

The numerical values for the angular frequencies ω_k and damping factors h_k are:

$\omega_0=2\pi f_0$ $\quad f_0=0.05$ Hz
$\omega_1=2\pi f_1$ $\quad f_1=5.0$ Hz
$h_0=0.707$
$h_1=0.623$
$h_2=0.223$
$h_3=0.901$

Substitution of $s=j\omega$ into Eq. (3) yields the complex gain-and-phase characteristics $H(j\omega)$ with gain $|H(j\omega)|$ and phase-shift $\varphi(\omega)$:

$$H(j\omega)=|H(j\omega)|\,e^{j\varphi(\omega)}=H_0(j\omega)\cdot H_1(j\omega). \tag{4}$$

Figure 1 shows the polar diagram of $H(j\omega)$. For an harmonic ground velocity $\hat{u}_0\exp(j\omega t)$ with amplitude $|\hat{u}_0|=1$ and phase-shift $\arg(\hat{u}_0)=0$ (represented by a unit vector along the real axis), the absolute value and argument of the complex vector $H(j\omega)$ give the amplitude and phase-shift of the BB-output voltage. $H(j\omega)$ intersects the 3-db circle at frequencies close to 0.05 Hz and 5.0 Hz.

The gain $|H(j\omega)|$ follows from Eq. (4) for $h_0=1/\sqrt{2}$ as

$$|H(j\omega)|=\frac{\omega^n/\omega_0^2}{[1+(\omega/\omega_0)^4]^{\frac{1}{2}}}\cdot\frac{1}{[1+(\omega/\omega_1)^{14}]^{\frac{1}{2}}} \tag{5}$$

$|H(j\omega)|$ is plotted in Fig. 2 for the BB-output for ground velocity with the gain factor $G_{0\,BB}=2{,}400$ V s/m. The low frequency values for the 3-db frequency and slope are 0.05 Hz and 12 db/octave, the high frequency values are 5.0 Hz and 42 db/octave. The

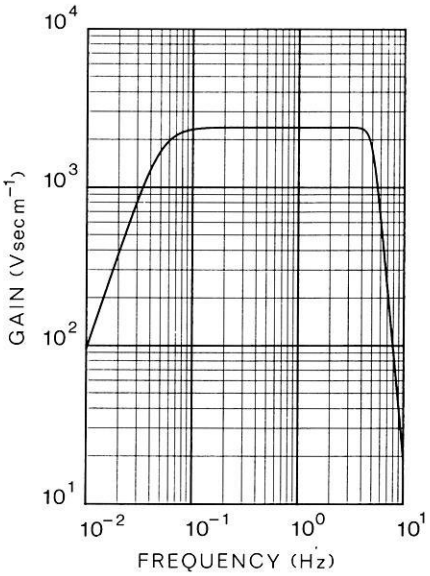

Fig. 2. Gain of BB-output for ground velocity of the Graefenberg seismograph system (gain factor $G_{0\,\mathrm{BB}}=2{,}400$ V s/m)

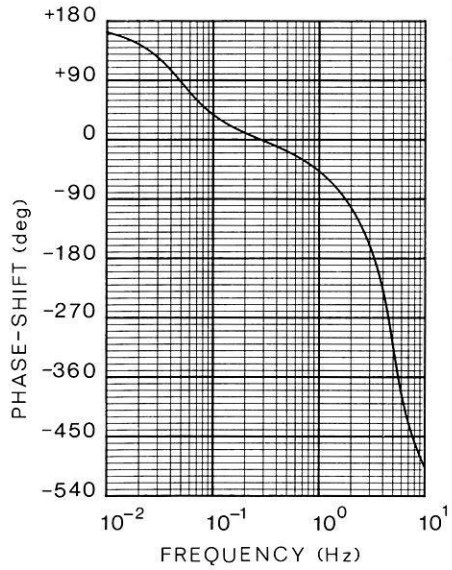

Fig. 3. Phase-shift of BB-output for ground velocity or LP-output for ground displacement of the Graefenberg seismograph system

effective bandwidth of $|H(j\omega)|$ defined by

$$W_\omega^2=4\pi^2 W_f^2=\frac{\int_0^\infty \omega^2 |H(j\omega)|^2 d\omega}{\int_0^\infty |H(j\omega)|^2 d\omega} \tag{6}$$

has the values $W_f=4.16$ Hz for $n=3$ in Eq. (4) and $W_f=3.00$ Hz for $n=2$. The phase-shift for $n=2$ is shown in Fig. 3.

The group-delay for the BB-output and LP-output is given by

$$\tau_G(\omega)=-\frac{d\varphi(\omega)}{d\omega}=\tau_{G_0}(\omega)+\tau_{G_1}(\omega) \tag{7}$$

where

$$\tau_{G_0}(\omega)=\frac{2h_0\,\omega_0(\omega^2+\omega_0^2)}{(\omega^2-\omega_0^2)^2+4h_0^2\,\omega_0^2\,\omega^2}$$

and

$$\tau_{G_1}(\omega)=\frac{\omega_1}{\omega^2+\omega_1^2}+2\omega_1\sum_{k=1}^{3}\frac{h_k(\omega^2+\omega_1^2)}{(\omega^2-\omega_1^2)^2+4h_k^2\,\omega_1^2\,\omega^2}.$$

The first term $\tau_{G_0}(\omega)$ corresponds to the seismometer $H_0(j\omega)$ in Eq. (4), the second term $\tau_{G_1}(\omega)$ is related to the antialiasing filter $H_1(j\omega)$. For $f<2$ Hz the group-delay τ_{G_1} is nearly constant ($\tau_{G_1}\approx 0.13$ s). For $f=0$ the overall group-delay $\tau_G(0)=4.65$ s.

The mean group-delay, defined by

$$\bar{\tau}_G=\frac{\int_0^\infty \tau_G(\omega)|H(j\omega)|^2 d\omega}{\int_0^\infty |H(j\omega)|^2 d\omega} \tag{8}$$

has the values $\bar{\tau}_{G\,\mathrm{BB}}=0.22$ s for $n=3$ in Eq. (4) and $\bar{\tau}_{G\,\mathrm{LP}}=0.25$ s for $n=2$, respectively. The overall group-delay is shown in Fig. 4.

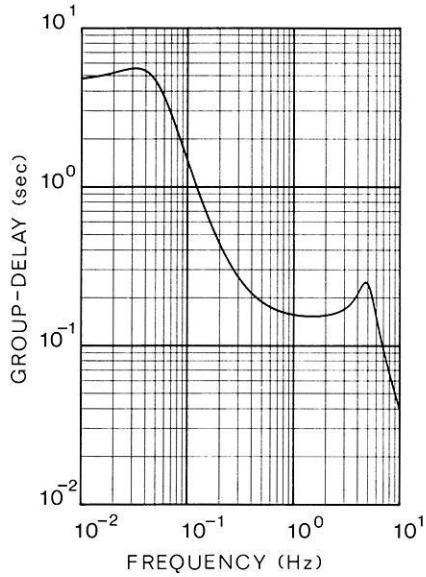

Fig. 4. Group-delay of the Graefenberg seismograph system

In the time domain the seismograph system can be described by the step response $h_\varepsilon(t)$ (response to unit step function $\varepsilon(t)$) or by the impulse response $h_\delta(t)$ (response to unit impulse function $\delta(t)$) for ground displacement or velocity, where $h_\delta(t)=d(h_\varepsilon(t))/dt$ and $h_{\delta\,\mathrm{BB}}(t)=d(h_{\delta\,\mathrm{LP}}(t))/dt$.

Figure 5 shows the response of the BB-output (LP-output) to a ground velocity (displacement) step function for the seismometer (Eq. (1)), the antialiasing filter (Eq. (2)) and the overall system (Eq. (3)). The leading edge of the step response is determined mainly by the antialiasing filter. The rise time from zero to maximum amplitude is $T_R=0.245$ s ($T_R\approx\tau_{G_1}(0)+1/2\ (1/(2f_1))$, f_1 upper 3-db frequency of antialiasing filter). The trailing edge is determined by the seismometer. The decay time

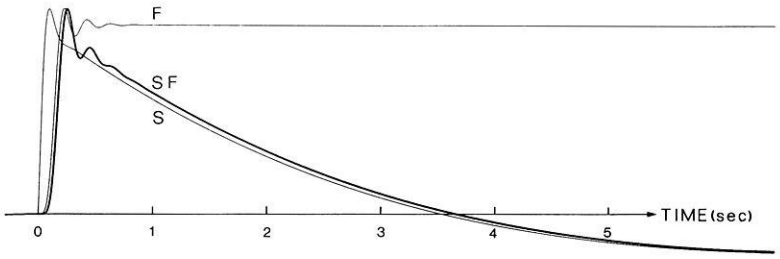

Fig. 5.
F Step response of antialiasing filter $H_F(s)$
S Step response of seismometer $H_S(s)$ (BB-output for ground velocity or LP-output for ground displacement)
SF Corresponding response of seismograph system $H(s)$

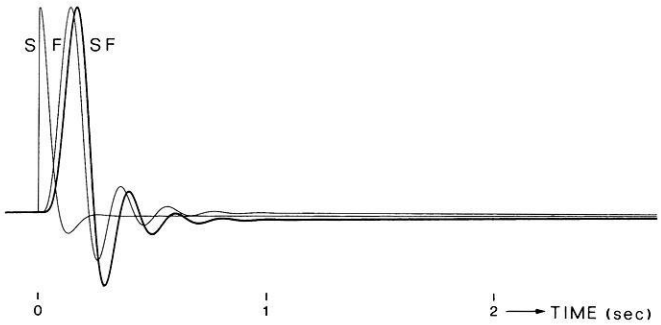

Fig. 6.
F Impulse response of antialiasing filter $H_F(s)$
S Impulse response of seismometer $H_S(s)$ (BB-output for ground velocity or LP-output for ground displacement)
SF Corresponding response of seismograph system $H(s)$

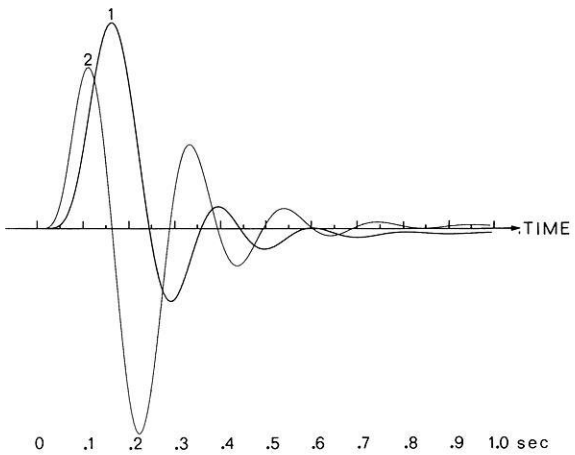

Fig. 7.
1 LP-output impulse response of seismograph system $H(s)$ for ground displacement
2 BB-output impulse response of seismograph system $H(s)$ for ground displacement
Response curves are normalized to maxima. The time axis is scaled in sampling intervals of $T=0.05$ s

from maximum to first zero is $T_D=3.455$ s ($T_D \approx 1/(2\pi f_0)$), f_0 lower 3-db frequency of seismometer for damping factor $h_0=0.707$ (T_D increases slightly with increasing damping factor).

Figure 6 shows the time derivatives of the response curves in Fig. 5, which are determined mainly by the antialiasing filter. For the ground displacement impulse response of LP-output the rise time to first maximum is $T_{R\,\mathrm{LP}}=0.165$ s and the time to first minimum $T_{\min\,\mathrm{LP}}=0.290$ s. The times to first and second zero are $T_{0\,1\,\mathrm{LP}}=0.245$ s and $T_{0\,2\,\mathrm{LP}}=0.351$ s, respectively.

Figure 7 shows in a larger time scale the ground displacement impulse responses for BB-output and LP-output. For the ground displacement impulse response of BB-output, the rise time to first maximum is $T_{R\,\mathrm{BB}}=0.115$ s and the time to first minimum is $T_{\min\,\mathrm{BB}}=0.220$ s. The times to first and second zero are $T_{0\,1\,\mathrm{BB}}=0.165$ s and $T_{0\,2\,\mathrm{BB}}=0.290$ s, respectively.

The consequences of the impulse response on the accuracy of arrival time measurement is elucidated in the last section. The significance of the displacement step response of LP-output for the estimation of the running time integral $\int_0^t f(\tau)\,d\tau$ for ground displacement $f(t)$ will be discussed in Paper II.

Digital simulation of seismograph systems

The accuracy of signal parameters extracted from seismograms depends on many factors: transfer function, dynamic range, resolution and time scale of the seismograph and recording system, signal and noise spectra and restoration algorithms. These relationships can be investigated best by numerical experiments with synthetic seismograms. For a wide class of input signals, the response of a seismograph system with a rational transfer function can be calculated analytically. If, for example, the Laplace transform of the input signal is also a rational function, the exact response is obtained by partial-fraction expansion. However, for input wavelets of short duration as well as theoretical seismograms and measured sampled data, a general solution by digital simulation techniques is preferred. These methods are based on linear digital filtering of sampled input signals and can be implemented on any minicomputer (Forster, 1980).

Simulation in the frequency domain

Basically, simulation in the frequency domain is performed by multiplying the Discrete Fourier Transform (DFT) of a finite length input sequence with $H(\omega_k)$ at N equidistant frequencies

$$\omega_k = 2\pi \frac{k \cdot f_S}{N} \qquad k=0, 1, \ldots, N-1 \tag{9}$$

and applying the inverse DFT to the product sequence of length N. Here $f_S=1/T$ is the sampling frequency and T the sampling interval. N must be chosen greater than or equal to the sum L_I+L_H, where L_I and L_H indicate the length of the input sequence and the length of the sampled impulse response $h_\delta(k \cdot T)$. Unlimited input sequences are segmented into blocks of length L_I

and the results of subsequent blockwise convolutions are added with an overlap of $N-L_I$ samples. With N a power of 2, the FFT-algorithms can be applied (fast convolution).

To simulate the response of a continuous system to a continuous signal with this method: *a*) the input signal must be bandlimited, *b*) the impulse response of $H(s)$ must be limited in time.

For the signals and systems considered here, both conditions can be fulfilled approximately provided that the sampling frequency f_S and the transform length N are chosen high enough.

Simulation in the time domain

Here Infinite Impulse Response (IIR) digital filters $H(z)$ with the following characteristics are considered: the error between the output $y_d(k)$ of the discrete system and the sampled response function $y_c(k \cdot T)$ of the continuous system should be minimized for a given driving function $x_c(t)$ and the corresponding sequence $x_d(k) = x_c(k \cdot T)$. Out of a large variety of methods, which are referenced by Renn (1976) and Schüssler (1981), we select those three $s \to z$ transformations where either the impulse response, step response or ramp response of the discrete and the continuous filter are identical at times $t_k = k \cdot T\,(k = 1, 2, 3, \ldots)$.

These $s \to z$ transformations, the impulse (IIT), step (SIT) or ramp (RIT) invariant transformation, yield the coefficients of difference equations by which the digital filter $H(z)$ will be realized.

The advantage of time domain simulation is that the impulse response $h_\delta(t)$ is not required to have a finite length.

Impulse invariant transformation

Starting with a partial-fraction expansion of $H(s)$ and, for the sake of simplicity, considering only simple poles and $\lim_{s\to\infty} H(s) = 0$ (for other cases, see Schüssler, 1981),

$$H(s) = \sum_{\nu=1}^{n} \frac{R_\nu}{s - s_{\infty\nu}} \tag{10}$$

where $R_\nu = \lim_{s\to s_{\infty\nu}} (s - s_{\infty\nu})\, H(s)$.

The impulse response is then given by

$$h_\delta(t) = \sum_{\nu=1}^{n} R_\nu e^{s_{\infty\nu} \cdot t} \cdot \varepsilon(t). \tag{11}$$

At the sampling points $t_k = k \cdot T$, the continuous impulse response $h_\delta(t)$ coincides with the impulse response sequence $h_I(k)$ of the desired discrete system

$$h_I(k) = h_\delta(kT) = \sum_{\nu=1}^{n} R_\nu (e^{s_{\infty\nu} \cdot T})^k\, \varepsilon_k \tag{12}$$

where ε_k is the step sequence ($\varepsilon_k = 0$ for $k < 0$ and $\varepsilon_k = 1$ for $k \geqq 1$).

With $z_{\infty\nu} = \exp(s_{\infty\nu} \cdot T)$, z-transformation of $h_I(k)$ leads to

$$H_I(z) = \sum_{\nu=1}^{n} R_\nu \frac{z}{z - z_{\infty\nu}}. \tag{13}$$

Here the subscript I stands for Impulse Invariant Transformation.

Sampling of $h_\delta(t)$ results in a periodic repetition of $H(j\omega)$:

$$H_I(e^{j\Omega}) = \frac{1}{T} \sum_{k=-\infty}^{+\infty} H\left(j\omega + j\frac{2\pi k}{T}\right) \tag{14}$$

where $\Omega = \omega T$.

Spectral overlapping will produce a frequency response $H_I(\exp(j\Omega))$ which may differ significantly from $H(j\omega)$.

Step invariant and ramp invariant transformation

The transfer functions $H_{ST}(z)$ and $H_R(z)$ are determined such that the step response or the ramp response of the discrete and the continuous system agree for $t_k = k \cdot T$. This condition leads to

$$H_{ST}(z) = \sum_{\nu=1}^{n} \frac{R_\nu}{s_{\infty\nu}} \cdot \frac{z_{\infty\nu} - 1}{z - z_{\infty\nu}} \tag{15}$$

for SIT and to

$$H_R(z) = -\sum_{\nu=1}^{n} \frac{R_\nu}{s_{\infty\nu}} + \sum_{\nu=1}^{n} \frac{R_\nu (z_{\infty\nu} - 1)}{s_{\infty\nu}^2 \cdot T} \cdot \frac{z - 1}{z - z_{\infty\nu}} \tag{16}$$

for RIT.

The invariance of either type holds not only for a single impulse function $\delta(t)$, step function $\varepsilon(t)$ or ramp function $\gamma(t)$ but also for combinations of time delayed input signals $\delta(t - k \cdot T)$, $\varepsilon(t - k \cdot T)$ or $\gamma(t - k \cdot T)$, which include all types of step functions or polygons.

For different input signals, discrepancies between the responses $y_c(k \cdot T)$ and $y_d(k)$ will be observed if the sampling theorem is not satisfied for the input signal and for the impulse response of the filter. In most cases of practical interest, the simulation error can be kept very low by choosing a sufficiently high sampling rate. The question, whether IIT, SIT or RIT produces a lower simulation error, can be answered for a given $H(s)$ only for certain classes of driving functions. Impulse Invariant Transformation proves to be best, if two conditions are met (Geisser, 1983): *a*) $X(s)$ is a rational function with simple poles, different from those of $H(s)$, *b*) $x_c(t)$ and $h_\delta(t)$ are continuously differentiable at $t = 0$.

The complete simulation program (Fig. 8) consists of a "design segment", which determines the coefficients of the digital filters $\hat{H}_2(z)$ and $\hat{H}_3(z)$ for a given continuous system $H(s)$, and a "filtering segment", which computes the output signal $y_v(k)$ for a given input $x_d(k)$.

The design may be based either on the coefficients of $H(s)$ or its poles and zeros. Residuals and poles could be prescribed as well. If they are not given in advance, they must be determined to perform the $s \to z$ transformation. After a transformation according to Eq. (13), (15) or (16), blocks of second order are constructed from the $(B_\nu z + A_\nu)/(z - z_{\infty\nu})$ by the combination of complex conjugate or two real terms. The resulting transfer function

$$H(z) = \sum_{i=1}^{M} \frac{d_{2i} z^2 + d_{1i} z + d_{0i}}{z^2 + c_{1i} z + c_{0i}} \tag{17}$$

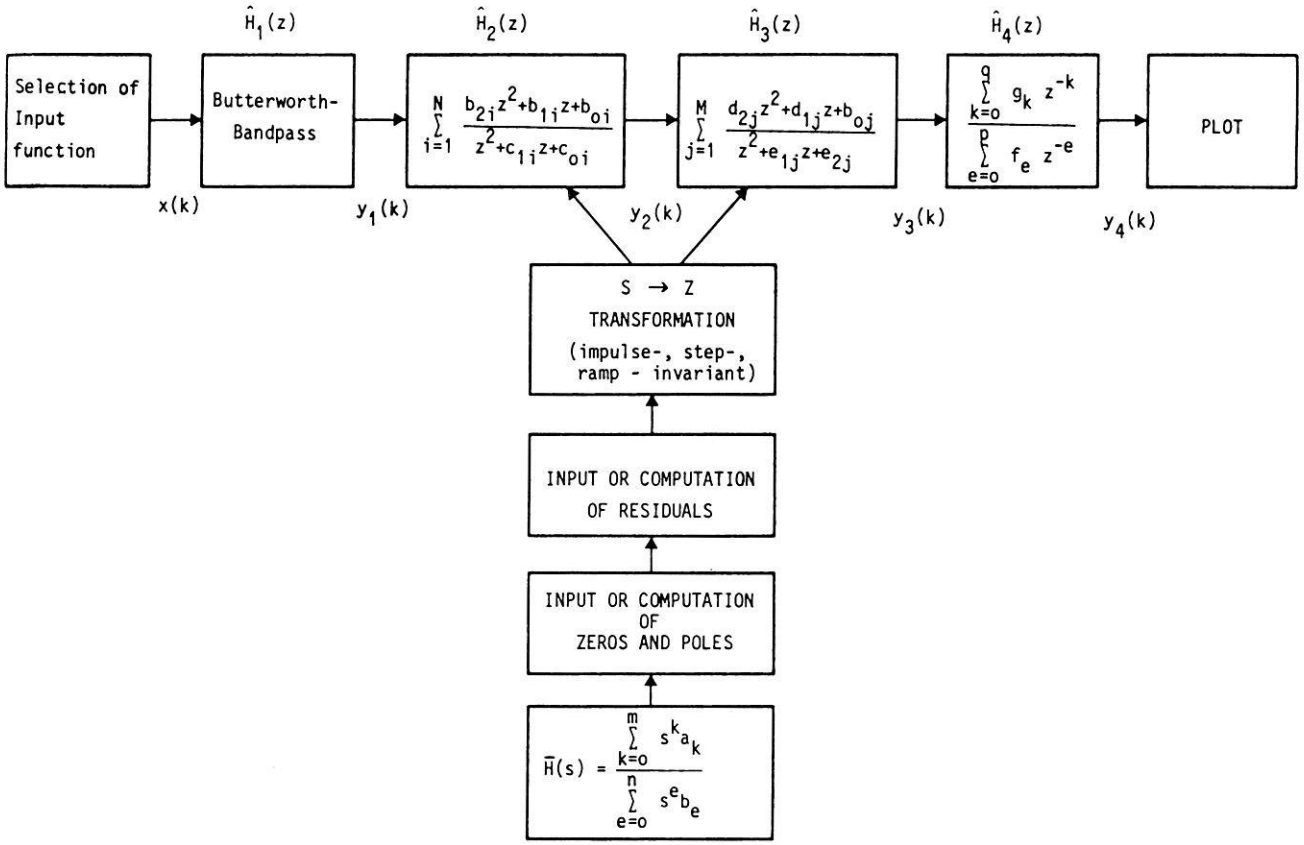

Fig. 8. Digital simulation of seismograph systems

leads to a digital filter in parallel form which is implemented by the following difference equations:

$$y_i(k) = -c_{1i} \cdot y_i(k-1) - c_{0i} \cdot y_i(k-2) + d_{2i} u(k) + d_{1i} u(k-1) + d_{0i} u(k-2) \quad i = 1, 2, \ldots, M \tag{18}$$

$$y(k) = \sum_{i=1}^{M} y_i(k). \tag{19}$$

The "filtering segment" includes further digital filters $\hat{H}_1(z)$ and $\hat{H}_4(z)$ for digital band limitation and restoration filtering, respectively.

All computations are done in double precision arithmetic to assure that truncation and rounding errors have little effect on the result for high sampling rates.

Time domain restoration

Arrival time

It is not possible to give a general definition of a seismic onset which can be used for the actual measurement of first arrival time and first motion sign from a sampled band-limited signal in the presence of noise. Signals propagating in a medium with absorption and dispersion can be considered to be wavelets, that is causal time functions ($f(t)=0$ for $t<0$) with finite energy $\left(\int_0^\infty f^2(t)\,dt < \infty\right)$. The Laplace transform of a wavelet is then analytic in a right half-plane. The discontinuity at the wavelet front $t=+0$ is called an onset of order p, if $f^{(p)}(+0)$ is the first nonzero derivative. The front velocity of the wavelet is determined by the asymptotic limit of the phase velocity for high frequencies. This follows from the Signal Front Theorem in Eq. (20). The sharpness of the wavelet front depends on the counteracting influences of dispersion and absorption as a function of distance and frequency. For short distances the absorption is small and the dispersion tends to sharpen the wavelet front. With increasing distance the effect of absorption becomes dominating and the wavelet front is correspondingly smoothed.

Using the wavelet model for body waves and applying the Signal Front Delay Theorem and the Initial Value Theorem (Papoulis, 1962), some general consequences about time delay and distortion of the wavelet leading edge by a seismograph system can be derived.

The Signal Front Delay Theorem states that the response of a linear causal system to a wavelet $f(t) \cdot \varepsilon(t)$ with arrival time $t_A = 0$ is a wavelet $u(t) \cdot \varepsilon(t - \tau_F)$ with onset time $t_S = \tau_F$. The signal front delay τ_F is given by the high frequency limit of the system phase-delay $\tau_P(\omega)$:

$$\tau_F = \lim_{\omega \to \infty} \tau_P(\omega) = \lim_{\omega \to \infty} \frac{\varphi(\omega)}{\omega}. \tag{20}$$

For seismograph systems with rational transfer functions $\tau_F = 0$, because $\varphi(\omega) \to$ constant as $\omega \to \infty$.

Given a wavelet $f(t)$ with onset order p and Laplace

Transform $F(s)$, the Initial Value Theorem states that

$$f^{(m)}(+0)=\lim_{s\to\infty} s^{m+1}F(s) \tag{21}$$

holds for all $m\leqq p$. Since $f^{(p)}(+0)=f_p$ is the first non-zero derivative, $F(s)$ has the asymptotic form

$$F(s)\sim f_p\cdot s^{-(p+1)} \tag{22}$$

as $s\to\infty$. The behavior of $f(t)$ near $t=+0$ then becomes

$$f(t)\sim\frac{f_p}{p!}t^p. \tag{23}$$

If this wavelet with onset order p is recorded by a seismograph system with transfer function

$$H(s)=\frac{\sum_{i=1}^{m} a_i s^i}{\sum_{k=1}^{n} b_k s^k}\qquad m\leqq n \tag{24}$$

then the Laplace Transform $U(s)=H(s)\cdot F(s)$ of the seismogram wavelet $u(t)$ has the asymptotic form

$$U(s)\sim\frac{a_m}{b_n}\cdot f_p\cdot s^{m-n-(p+1)} \tag{25}$$

as $s\to\infty$. The behavior of the seismogram near the onset time $t=+0$ is then

$$u(t)\sim\frac{a_m}{b_n}\cdot\frac{f_p}{(n-m+p)!}t^{n-m+p}. \tag{26}$$

Thus the seismograph system increases the onset order of the input wavelet by $n-m$.

According to the Signal Front Delay Theorem, there is no time shift between the signal front arrival time and the seismogram onset time. The precision of visual detection of the onset depends on curvature and rise time of the seismogram's leading edge as well as on noise level and recording scale. The sharpest possible onset, the response to a δ-impulse in ground displacement (upper cutoff frequency $f_c=\infty$), is shown in Fig. 7 for the LP-output and BB-output. For LP-output, $h_{\delta\,\mathrm{LP}}(t)\sim t^6$ as $t\to 0$ (Eqs. (22) and (23)), since $H_{\mathrm{LP}}(s)\sim s^7$ as $s\to\infty$ (Eq. (3)). The rise time from zero to 1% of maximum amplitude is $T_{R\,0.01\,\mathrm{LP}}\approx T$ (sampling interval $T=0.05$ s). For BB-output, $h_{\delta\,\mathrm{BB}}(t)\sim t^5$ and $T_{R\,0.01\,\mathrm{BB}}\approx 0.5\,T$.

Figure 9 again shows for the BB-output the displacement impulse response as well as the synthetic seismograms for input signals $f(t)=t\exp(-a\cdot t)$ (order of onset $p_f=1$) with $f_c=1$ Hz and $f_c=0.2$ Hz, respectively. Since $F(s)=(s+a)^{-2}\sim s^{-2}$ as $s\to\infty$, $u_{\mathrm{BB}}(t)\sim t^7$ as $t\to 0$. Thus, an apparent delay in the arrival time of the order of magnitude 0.1 s may be introduced for a noise level of 10% of maximum first motion amplitude.

As an example, the Figs. 10 and 11 show the arrival time measurement for the P_n-wave of the Albstadt earthquake. For the BB-recording, the first maximum is about 35 db above noise level and forms the strongest onset yet observed at the Graefenberg Observatory.

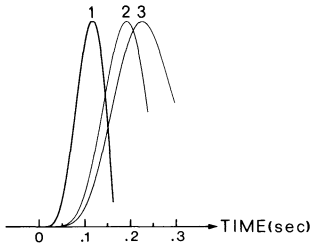

Fig. 9.
1 BB-output impulse response for ground displacement
2 Simulated response of BB-output for displacement input $t\cdot\exp(-a\cdot t)\cdot\varepsilon(t)$ ($\varepsilon(t)$ unit step function). Upper 3-db frequency of input spectrum $f_c=1$ Hz ($a=9.76\,\mathrm{s}^{-1}$)
3 Corresponding response for $f_c=0.2$ Hz ($a=1.95\,\mathrm{s}^{-1}$)

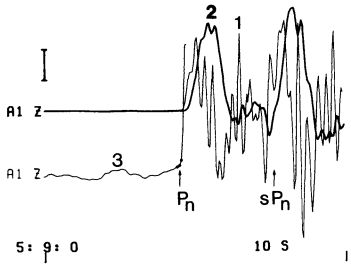

Fig. 10. Broad-band recordings of the P_n-sP_n wave group for the Albstadt (Swabian Jura) earthquake on 3. September 1978 (05 h 08 m 31.8 s; 48.28° N, 9.03° E, 6.6 km depth, 5.9 M_L, 224 km distance).
1 BB-output proportional to ground velocity (marked amplitude scale unit $\triangleq 9$ µm/s)
2 Recording proportional to ground displacement, calculated from BB-output (scale unit $\triangleq 1.2$ µm)
3 BB-output (scale unit $\triangleq 0.06$ µm/s).
The arrow points to the sampled time 05 h 09 m 04.55 s, the dots indicate three successive samples

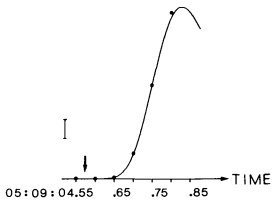

Fig. 11. Sampled values for the leading edge of the P_n-wave group in Fig. 10 (scale unit $\triangleq 1.2$ µm/s). The solid line shows the simulated BB-output response for a half-cycle displacement sinusoidal wave (frequency 0.33 Hz, onset time marked by arrow)

The arrival time is 05 h 09 m 04.55 ± 0.05 s. The ground displacement of the P_n-wave calculated by integration of the BB-seismogram can be approximated by a half-cycle sine wave with frequency 0.33 Hz. Figure 11 shows the corresponding synthetic seismogram of the BB-output. The best fit with the sampled data is obtained for the arrival time 05 h 09 m 04.575 ± 0.025 s of the input sine wavegroup. Hence, for this special case the arrival time can be determined with an accuracy of ± 0.025 s (half sampling interval).

To clarify some common misconceptions, a few remarks about the meaning of group-delay for broad-

band signals may be useful. The group-delay is usually used to refer to the envelope delay of a narrow-band signal (Papoulis, 1962). One application is the measurement of the group velocity dispersion of surface waves in the time domain. A generalization to broad-band signals $f(t)$ is the signal-delay, defined by

$$\tau_{f^2}=\frac{\int_0^\infty t\cdot f^2(t)\,dt}{\int_0^\infty f^2(t)\,dt}. \tag{27}$$

Substituting for $f(t)$ the impulse response $h_\delta(t)$ yields

$$\tau_{h_\delta^2}=\bar{\tau}_G \tag{28}$$

where $\bar{\tau}_G$ is the mean group-delay of the seismograph system, defined in Eq. (8) (Morgenstern, 1971). $\tau_{h_\delta^2}$ can be interpreted as the delay of the center of energy of $h_\delta(t)$. For low pass systems with $|H(0)|\neq 0$ the delay of the center of inertia

$$\tau_{h_\delta}=\int_0^\infty t\cdot h_\delta(t)\,dt\Big/\int_0^\infty h_\delta(t)\,dt=\tau_G(0)$$

(Kaufmann, 1959). The signal-delay for arbitrary wavelets is discussed by Mecklenbräuker (1982). Denoting the group-delay of the input signal $f(t)$ as $\tau_{Gf}(\omega)$, the signal-delay of the seismogram $u(t)$ is given by

$$\tau_{u^2}=\frac{\int_0^\infty [\tau_{Gf}(\omega)+\tau_G(\omega)]\cdot|F(j\omega)|^2\cdot|H(j\omega)|^2\,d\omega}{\int_0^\infty |F(j\omega)|^2\cdot|H(j\omega)|^2\,d\omega} \tag{29}$$

Thus, for a given seismograph system, the signal-delay of the seismogram depends on the shape of the input wavelet. For wavelets $f(t)=t\cdot\exp(-a\cdot t)$ with upper 3-db frequencies $f_c=0.102\cdot a$ the signal-delay of the seismograph system $\tau_S=\tau_{u^2}-\tau_{f^2}$ can be given as a function of f_c. In the interval $0.1\,\text{Hz}<f_c<1.0\,\text{Hz}$, $\tau_{S\,\text{LP}}(f_c)$ decreases from $\tau_{S\,\text{LP}}(0.1)=1.72$ s to $\tau_{S\,\text{LP}}(1.0)=0.48$ s. For the BB-output $\tau_{S\,\text{BB}}(f_c)$ increases from $\tau_{S\,\text{BB}}(0.1)=-0.91$ s to $\tau_{S\,\text{BB}}(1.0)=0.07$ s. The group-delay is irrelevant in determining first arrival times.

First motion sign

The first motion sign of the input wavelet $f(t)$ with p-order onset is given by f_p in Eq. (22). If the seismograph system is calibrated such that in Eq. (24) a_m/b_n is positive, the first motion sign of the seismogram in Eq. (26) is also given by f_p. Therefore, a seismograph system with a rational transfer function cannot change the first motion sign of the input wavelet.

Quite often body wave signals are superpositions of low frequency and high frequency pulses. In this case, broad-band outputs proportional to ground displacement and velocity or narrow-band short and long period seismograph systems can separate these superimposed wavegroups. Even if the low frequency wavelet and the first high frequency pulse have the same arrival times but different first motion signs, the direction of

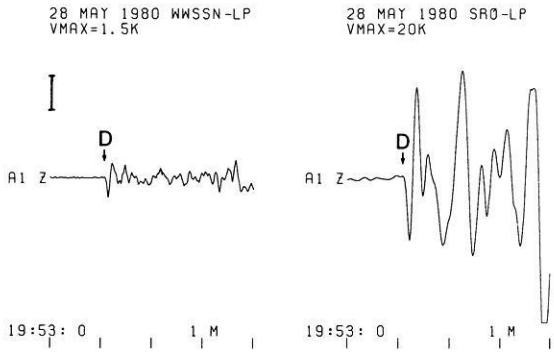

Fig. 12. WWSSN-LP and SRO-LP P-wave seismograms with negative first motion sign for a Sicilian earthquake on 28. May 1980 (19 h 51 m 19.3 s; 38.48° N, 14.25° E, 5.5 M_L, 11.4° distance), simulated from BB-output of array station $A1-Z$. Maximum magnifications $V_{\max}$ refer to marked amplitude scale of 1 cm. Marked time scale units $\hat{=}$ 1 min

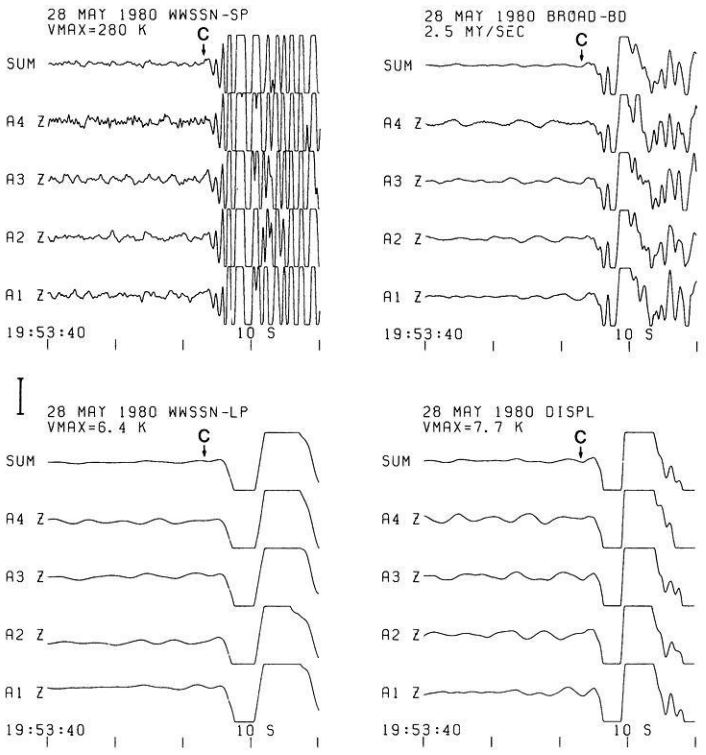

Fig. 13. P-wave recordings for the earthquake in Fig. 12 for several array stations with beams (SUM), indicating positive first motion signs for the narrow band and broad-band recordings. Maximum magnifications $V_{\max}$ refer to marked amplitude scale of 1 cm. Marked time scale units $\hat{=}$ 10 s

first motion is the same in all seismograms and is not related to some characteristic frequency of the seismograph system. The actual reading may depend on the signal-to-noise ratio. When the latter is good, the first motion can be interpreted as short period compression and long period dilatation or vice versa. The Figs. 12 to 14 show typical examples.

In Fig. 12, the WWSSN-LP and SRO-LP seismograms for an earthquake in Sicily are simulated from broad-band data using standard amplitude and time scales. In both cases, the first motion sign appears to be

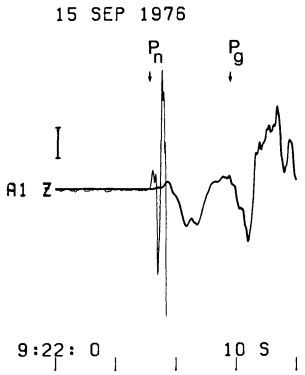

Fig. 14. Recordings of the $P_n - P_g$ wave group for a Friuli earthquake on 15. September 1976 (09 h 21 m 19.1 s; 46.32° N, 13.13° E, 5.9 M_L, 401 km distance). Marked time scale units $\triangleq 10$ s
1 Simulated WWSSN-SP seismogram ($V_{max} = 93$ K for 1 cm marked amplitude scale) with positive first motion sign (short period compression)
2 Broad-band recording proportional to ground displacement (calculated from BB-output, scale unit $\triangleq 39$ μm) with negative first motion sign (long period dilatation)

negative (long period dilatation). When the amplitude and time scales are greatly magnified, as in Fig. 13, the first motion sign is definitely positive on both broad-band and narrow-band seismograms.

Figure 14 shows an analogous example for a Friuli earthquake. Here the first motion sign of the P_n - wave of the simulated WWSSN-SP seismogram is positive (short period compression), whereas the sign of the broad-band recording proportional to ground displacement can be interpreted as being negative (long period dilatation), neglecting the tiny initial pulse with positive sign.

The measurement of arrival time and first motion sign is dependent only on the restoration of the signal front. The estimation of various functionals of the input signal such as running time integrals of true ground displacement and velocity or spectral amplitudes for the determination of magnitude and moment is discussed in Paper II.

Conclusion

The Signal Front Delay Theorem states that the linear distortions caused by the seismograph system will not introduce a delay in the onset time of the input wavelet. However, the steep slope of the transfer function at high frequencies, given by the antialiasing filter, will flatten the curvature of the wavelet leading edge. In the case of superimposed noise, the wavelet onset may appear to be delayed. The delay depends mainly on the upper corner frequency of the input wavelet and the signal-to-noise ratio. For example, for a signal to noise ratio of 20 db, the BB-output of the Graefenberg seismograph system has an apparent delay on the order of 0.05 s for $f_c > 5\ Hz$ and 0.1 s for $0.2 < f_c < 1$ Hz. If the signal-to-noise ratio is much higher, fitting the leading edge of the seismogram with synthetic responses can reduce the arrival time error to less than 0.05 s (sampling interval).

A seismograph system with a rational transfer function cannot change the first motion sign of the input wavelet. The reading of different short and long period first motion signs is meaningful only for overlapping low and high frequency wavelets. From broad-band recordings the first motion signs of the superimposed pulses of different frequencies can be determined separately by simulating wide-band seismograms proportional to ground displacement and velocity, or narrow-band long and short period seismograms.

Acknowledgments. We are greatly indebted to E. Wielandt for critically reading the manuscript and for many cogent comments. We are also grateful to M. Hellweg for translation assistance and several suggestions. O. Sembritzky provided programming assistance. The Graefenberg array is part of the Bundesanstalt für Geowissenschaften und Rohstoffe (Federal Institute for Geosciences and Natural Resources) and is supported by the Deutsche Forschungsgemeinschaft (German Research Council).

References

Forster, H.: Simulationsprogrammsysteme SIMPRO und PLL. Ausgewählte Arbeiten über Nachrichtensysteme Nr. 45, Lehrstuhl für Nachrichtentechnik, Universität Erlangen, 1980

Geisser, H.: Simulation kontinuierlicher Systeme. Studienarbeit am Lehrstuhl für Nachrichtentechnik, Universität Erlangen, 1983

Harjes, H.-P., Seidl, D.: Digital recording and analysis of broad-band seismic data at the Graefenberg (GRF) - array. J. Geophys. **44**, 511–523, 1978

Kaufmann, H.: Dynamische Vorgänge in linearen Systemen der Nachrichten- und Regelungstechnik. R. Oldenburg, München, 1959

Mecklenbräuker, W.: Gruppenlaufzeit und Laufzeit der Signalenergie in kausalen linearen Systemen. AEÜ **36**, 356–358, 1982

Morgenstern, G.: Gruppenlaufzeit und Impulslaufzeit. AEÜ **25**, 393–395, 1971

Papoulis, A.: The Fourier integral and its applications. New York: McGraw-Hill 1962

Renn, H.P.: Untersuchungen über Zeitbereichsverfahren zur digitalen Simulation von linearen zeitinvarianten Systemen. Ausgewählte Arbeiten über Nachrichtensysteme Nr. 26, Lehrstuhl für Nachrichtentechnik, Universität Erlangen, 1976

Robinson, E.A.: Random wavelets and cybernetic systems. London: Charles Griffin & Co. Ltd.

Schüssler, H.-W.: A signalprocessing approach to simulation. Frequenz **35**, 174–184, 1981

Seidl, D.: The simulation problem for broad-band seismograms. J. Geophys. **48**, 84–93, 1980

Wielandt, E., Streckeisen, G.: The leaf-spring seismometer: Design and performance. Bull. Seismol. Soc. Am. **72**, 2349–2367, 1982

Received June 28, 1983; Revised version October 13, 1983
Accepted October 13, 1983